THE JOURNAL OF PHYSICAL CHEMISTRY B

Article

pubs.acs.org/JPCB

Structure and Dynamics of Ionic Micelles: MD Simulation and Neutron Scattering Study

B. Aoun,[†] V. K. Sharma,[‡] E. Pellegrini,[†] S. Mitra,[‡] M. Johnson,[†] and R. Mukhopadhyay*[,‡]

[†]Institut Laue-Langevin, BP 156, 6, rue Jules Horowitz, 38042 Grenoble Cedex 9, France

[‡]Solid State Physics Division, Bhabha Atomic Research Centre, Mumbai 400 085, India

Supporting Information

ABSTRACT: Fully atomistic molecular dynamics (MD) simulations have been carried out on sodium dodecyl sulfate (SDS), an anionic micelle, and three cationic (C_nTAB; n = 12, 14, 16) micelles, investigating the effects of size, the form of the headgroup, and chain length. They have been used to analyze neutron scattering data. MD simulations confirm the dynamical model of global motion of the whole micelle, segmental motion (headgroup and alkyl chain), and fast torsional motion associated with the surfactants that is used to analyze the experimental data. It is found that the solvent surrounding the headgroups results in their significant mobility, which exceeds that of the tails on the nanosecond time scale. The middle of the chain is found to be least mobile, consolidating the micellar configuration. This dynamical feature is similar for all the ionic micelles investigated and therefore independent of headgroup form and charge and chain length. Diffusion constants for global and segmental motion of the different micelles are consistent with experimentally obtained values as well as known structural features. This work provides a more realistic model of micelle dynamics and offers new insight into the strongly fluctuating surface of micelles which is important in understanding micelle dispersion and related functionality, like drug delivery.

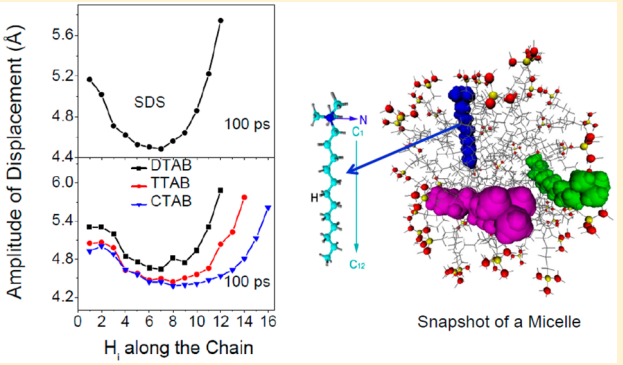

INTRODUCTION

Amphiphilic molecules such as surfactants and lipids exhibit a rich variety of phases in aqueous solution. They undergo self-association under specific conditions to form aggregates such as micelles, vesicles, bilayers, wormlike micelles, etc. The geometry of the aggregates is a result of a delicate balance between two opposing forces. The attractive tail−tail hydrophobic interaction provides the driving force for the aggregation of surfactant molecules, while the electrostatic repulsion between the headgroup puts a lower limit on the size that a micelle can attain. Self-assembled micellar aggregates have been the subject of intense interest for several decades, both from a fundamental physical-chemistry point of view and because of their widespread applications in detergent, cosmetic, pharmaceutical, and food industries.[1] In addition, the separation of the hydrophobic and hydrophilic regions and the existence of an interface (polar headgroup and water) make them appropriate model systems for biological membranes. While understanding of structure and macroscopic behavior seems to converge, the dynamical behavior of these assemblies and their correlation with microstructure is of current interest. Local dynamics in such assemblies are important in understanding various functions such as release of solubilized drugs, micellar breaking, and synthesis of nanoparticles with most relevant processes being initiated at the micelle surface.[2]

Dynamical processes in micelles are complex and include multiple relaxation processes on local and global scales. They can be studied experimentally via dynamic light scattering (DLS),[3] nuclear magnetic resonance (NMR),[4,5] fluorescence spectroscopy,[6,7] and quasi-elastic neutron scattering (QENS)[8−13] techniques. DLS is limited in time scale to the measurement of global diffusion of micelles. NMR and fluorometric measurements of micellar solutions demonstrate that the segmental mobility of the chains of micelle forming molecules increases from the polar head to the nonpolar tail.[5,7] On the basis of these observations, the perceived image of the micelles is that of a massive headgroup which is relatively immobile at the micellar surface and the alkyl chains which are more mobile in the hydrophobic interior. Local dynamics of various ionic micelles[9−13] have been studied using QENS techniques to test the naive model of the surfactant dynamics in which the mobility increases from the headgroup at the micelle surface to the tail in the hydrophobic interior. A similar model is widely used to explain dynamics of phospholipid-based membranes[14−16] and vesicles.[17] However, while essential information is provided by QENS experiments, data analysis

Received: January 2, 2015
Revised: March 24, 2015

DOI: 10.1021/acs.jpcb.5b00020
J. Phys. Chem. B XXXX, XXX, XXX−XXX

may sometimes become difficult due to the presence of a number of dynamical processes and their correlations.

Molecular dynamics (MD) simulations cover the same length and time scales as QENS and are needed to provide a complete picture of the relaxation processes in these systems. MD simulation has been widely used to explore the structure and dynamical behavior of micelles,[18−27] lipid membranes,[14,16,28−30] etc. In this work, MD simulations have focused on the internal, segmental dynamics of the micelles and their relation to microstructure. They have been used to analyze QENS data. The results challenge the perceived idea of the micelle structure−dynamics relation, indicating that the surface layer fluctuates significantly, to the extent that the dynamical amplitude of the headgroup is comparable to or even bigger than that of the tails, depending on the time scale. This finding is of considerable interest given the applications of micelles, since the surface layer is the interface with the solvent where function-related processes, like micellar decomposition and release of solubilized drugs, are initiated.[2]

EXPERIMENTAL DETAILS

A 0.3 M micellar solution was prepared separately for sodium dodecyl sulfate (SDS) and DTAB samples in D_2O (99.9% atom D purity) for both surfactants. The neutron scattering experiments have been carried out using the time-of-flight spectrometer IN5 at the Institute Laue Langevin, Grenoble, France,[31] and the inverted geometry, backscattering spectrometer IRIS[32] at the ISIS pulsed neutron source, Didcot, U.K. IN5 was operated with an incident wavelength of 6 Å providing an energy resolution of $\Delta E = 60$ μeV (full width at half-maximum, fwhm). IRIS was operated with the 002 pyrolytic graphite analyzer providing an energy resolution of $\Delta E = 17.5$ μeV fwhm, and with the energy transfer range from −0.3 to 1.2 meV (in the offset mode). The wave-vector transfer (Q) range covered was 0.5−1.8 Å^{-1}. The samples were placed in an annular aluminum can with an internal spacing of 1 mm, giving no more than 10% scattering, thus avoiding multiple scattering. QENS measurements were performed at 300 K. The scattering contribution from D_2O, determined from a QENS measurement of D_2O, was subtracted from that of the micellar solution.

MOLECULAR DYNAMICS SIMULATION DETAILS

Fully atomistic MD simulations have been performed on a variety of ionic micelles in order to explore the effects of the size and form of the headgroup and the tail length. An anionic micelle, sodium dodecyl sulfate (SDS; $C_{12}H_{25}OSO_3^-Na^+$), and a series of cationic n-alkyl trimethylammonium bromide (C_nTAB; $C_nH_{2n+1}N^+(CH_3)_3Br^-$ with n = 12 (DTAB), 14 (TTAB), and 16 (CTAB)) with varied chain length have been selected for this purpose. The initial micelle structure was constructed from surfactant molecules in an all-*trans* conformation, assembled in a three-dimensional star-like configuration with the appropriate number of surfactant molecules taken from the literature. Water was added to the initial micelle model in a cubic, periodic box but excluded from the sphere occupied by the surfactant molecules, to reproduce the known concentration.

For example, to build an initial $C_{12}TAB$ (dodecyl trimethylammonium bromide: DTAB) micellar structure, 50 linear DTAB molecules were assembled in a cubic box which was then populated with 22 016 water molecules in order to achieve the 0.1 M concentration of DTAB. The number of DTAB molecules was chosen from the most probable mean aggregation number for DTAB micelles at room temperature found experimentally.[33] The number of surfactants and water molecules used for C_nTAB[33] and SDS[34] are given in Table 1.

Table 1. Numbers of Surfactant and Water Molecules Used to Build Different Micellar Systems

sample	number of surfactants	number of water molecules
SDS	60	11637
$C_{12}TAB$ (DTAB)	50	22016
$C_{14}TAB$ (TTAB)	84	31552
$C_{16}TAB$ (CTAB)	140	30037

MD simulations were carried out using the NAMD simulation software[35] with CHARMM 22 force-field parameters and charges for surfactant molecules and the TIP3P water model.[36] The equations of motions were integrated with a time step of 1 fs for all the interactions. The electrostatic interactions were calculated using the particle mesh Ewald algorithm with a grid spacing of 1 Å. Pressure was controlled by a Langevin piston with a target of 1 bar.

Geometry optimization, of the initial micellar model described above, followed by equilibration MD in an NPT ensemble allowed the surfactant molecules to relax and pack together. Approximately 1 ns is required to produce a dense hydrophobic tail region, but equilibration simulations were run for at least 10 ns. Since MD simulations can be run for longer times, we checked the convergence of the equilibration simulations for SDS. They were extended up to 75 ns and analyzed after 10, 25, 50, and 75 ns—no significant differences were observed between these results.

The analysis of the MD simulations is performed on production runs in which frames (structures) of the MD run are saved on a time scale corresponding to the experimental time scale, which in turn is determined by the energy resolution of the spectrometers. In this work, the two spectrometers, IRIS at ISIS and IN5 at ILL, have a resolution of 17 and 60 μeV (fwhm), respectively, corresponding to time scales of ∼100 and ∼30 ps. Structures were therefore saved every 5000 simulation steps, that is, every 5 ps. The length of the production runs is chosen to give adequate sampling of the structure and dynamics on the experimental time scale. Two ns simulations, composed of 400 simulation frames, were therefore chosen for the production runs.

All MD trajectories were analyzed using the nMoldyn[37] software. In particular, global translations, relevant to diffusion of whole micelles, are determined from the micelle center-of-mass coordinates. To study internal dynamics, global translations and rotations have to be removed, the latter being achieved by fitting the instantaneous structure of the micelle at a particular time onto the previous structure.[38] This results in a global-motion-filtered trajectory.

RESULTS AND DISCUSSION

Structure of Micelles. The MD simulations performed in the context of this work reproduce the established structural features of micelles.[22−26] A snapshot for DTAB micelle is shown in Figure 1. Formation of the DTAB micelle in a bath of water molecules is evident from the snapshot shown in Figure 1a. Surfactant alkyl chains composed of CH_2 groups are found in different conformations in the micelle. One molecule in fully *trans* configuration oriented roughly toward the center of the

DOI: 10.1021/acs.jpcb.5b00020
J. Phys. Chem. B XXXX, XXX, XXX−XXX

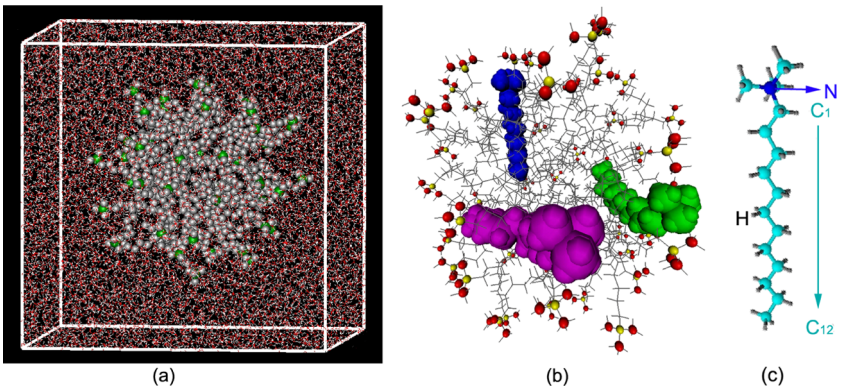

Figure 1. (a) Snapshot of DTAB micelle surrounded by water molecules. (b) DTAB micelles where few monomers with different conformations are marked in color after removing the water molecules for clarity. (c) Schematic of a DTAB monomer in fully *trans* configuration.

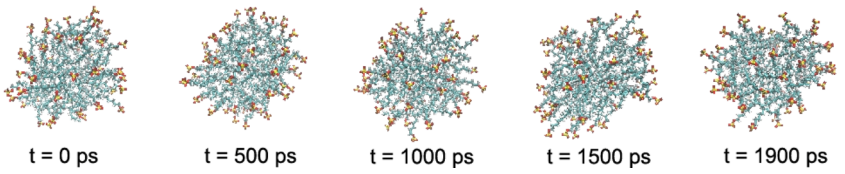

Figure 2. Snapshots of SDS micelles at different times during a simulation time of 2 ns.

micelle, one tangential to the micellar surface, and the other with a few gauche conformations are highlighted in Figure 1b. The DTAB molecule in fully *trans* configuration is shown in Figure 1c to indicate the atomic numbering. C_1−C_{12} are the carbon atoms in the alkyl chain. C_1 corresponds to the carbon atom near the headgroup, and C_{12} is the terminal carbon corresponding to the tail end. Snapshots of the SDS micelle at different times are shown in Figure 2, revealing the slightly nonspherical micellar shape. Extracting the principal axes of the ellipsoid from the global-motion-filtered trajectory allows the time-dependent eccentricity to be calculated (see the Supporting Information and ref 25)—it has an average value of ∼10% and shows several fluctuations during 2 ns.

Figure 3 shows the distribution of different molecular segments (headgroup and CH_2 units) as a function of their distances from the center of mass (COM) of the micelle for SDS and DTAB micelles. As the distance from the headgroup increases, the segment distance-to-COM distributions broaden. C_{12} has the largest distribution (0−20 Å), indicating that the tail can exist anywhere between the COM and the surface of the micelle. An interfacial layer of about 10 Å thickness, corresponding to the fwhm of the headgroup distance-to-COM distribution, can be defined, in which solvent can surround the headgroups and penetrate to a limited extent into the hydrophobic core, which is water-free inside a radius of ∼13 Å. The shape fluctuations, illustrated in Figure 2, contribute a small broadening to the distributions shown in Figure 3. For example, the maximum value of the headgroup distribution will be about 10% bigger compared to a spherical micelle. The micelles therefore present a rough, hydrated surface of ∼10 Å thickness composed of headgroups, water molecules, counterions, and some hydrophobic tails and a hydrophobic core of radius ∼13 Å.

Similar distributions for four, randomly selected, surfactants are shown in Figure 4 for the DTAB micelle for the tail end

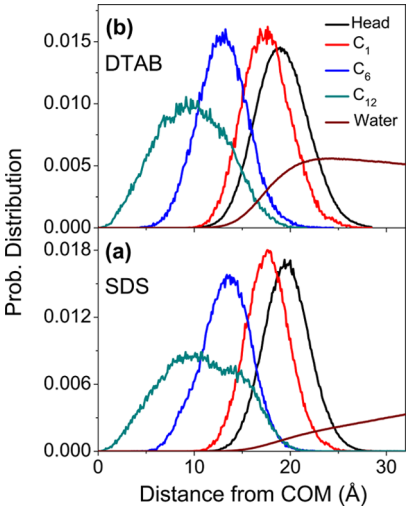

Figure 3. Probability distribution of water and segmental distances of monomer with respect to the COM for (a) SDS and (b) DTAB micelle.

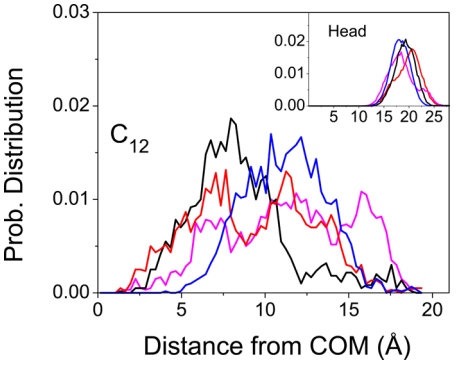

Figure 4. Probability distribution for C_{12} for four different DTAB monomers in the micelle. The localized motion of the headgroup (N atom) is shown in the inset.

DOI: 10.1021/acs.jpcb.5b00020
J. Phys. Chem. B XXXX, XXX, XXX−XXX

(C_{12}) and head, which therefore depict the distances covered by these segments of the surfactant molecules with respect to the center of mass over the 2 ns simulation time. The distribution of C_{12} spreads over 0−20 Å, while the headgroup is found to be distributed over 12−28 Å for all the monomers. The distributions for the tails of individual surfactants are about as large as the average distribution (shown in Figure 3), indicating that the tails can move from the center of the micelle to the surface or vice versa during 2 ns. In contrast, the movement of headgroups is clearly localized near the micellar surface. Similar dynamics are observed for all micelles.

Global Diffusion. The diffusion coefficient for the whole micelle, D_s, can be obtained from the mean square displacement (MSD) of COM trajectories using Einstein's relation:

$$D_s = \frac{1}{6t}\langle |r_{cm}(t + t_0) - r_{cm}(t_0)|^2 \rangle \quad (1)$$

The slope of the MSD vs time curve determines the diffusion constant, D_s. Figure 5 shows the center of mass (COM) MSD

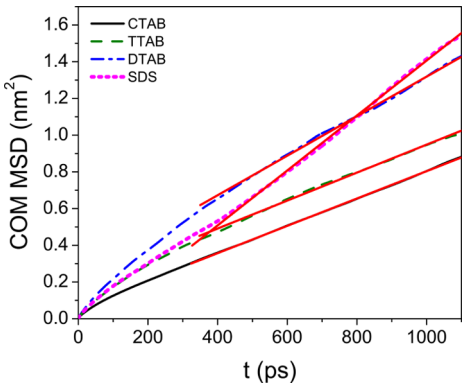

Figure 5. Plot of mean square displacement (MSD) of center of mass with time for C_nTAB micelles and SDS micelles. The diffusion coefficients are extracted from the linear fit (in the range 400−1000 ps, as shown in red) according to eq 1.

curves for C_nTAB and SDS micelles at 300 K. In the time dependence of the MSD for a dense colloidal suspension like micelles, generally there are three regimes. At very short time, since the particles are not interacting with each other, the displacement can be written as, $\Delta \mathbf{r}_{cm} = \mathbf{v}t$, where $\mathbf{v}$ is the velocity of the micelle and t is the time. In this case (ballistic regime), the MSD is proportional to $|\Delta r_{cm}|^2 \sim v^2t^2$, that is, to t^2. In the intermediate regime, the MSD shows a subdiffusive behavior. This is due to the cage effect; i.e., particles are trapped in transient cages formed by their neighbors, and thus cannot diffuse freely through the sample. In this case, mean square displacement is proportional to $|\Delta r_{cm}|^2 \sim t^{\alpha}$, where $\alpha < 1$. However, at long times (diffusive regime), the cages rearrange, and particles have lost any "memory" of their initial positions and are performing a random walk freely through the sample according to the Einstein equation (eq 1). Therefore, to estimate the diffusion constant, the slope from the MSD−time curve has to be determined at long enough time. Figure 5 shows that, for CTAB, TTAB, and DTAB, the subdiffusive regime extends up to 400 ps, and the diffusion constants for CTAB, TTAB, and DTAB micelles are determined from the gradient in the range from 400 to 1000 ps, as shown. In recent publications,[9−12] we have also reported the global diffusion of micelles obtained from neutron scattering experiments on this ~100 ps time scale. The experimentally observed, global diffusion of the micelles[11,12] is comparable with these simulations, as can be seen from the respective diffusion coefficients given in Table 2. It is to be noted that the global

Table 2. Diffusion Coefficients of C_nTAB and SDS Micelles as Obtained from MD Simulation and Experimen at T = 300 K

	D_s ($\times 10^{-6}$ cm^2/s) MD simulation	D_G ($\times 10^{-6}$ cm^2/s) QENS experiment
SDS	2.3 (±0.4)	2.6 (±0.2)[9]
DTAB	1.8 (±0.3)	2.9 (±0.3)[11]
TTAB	1.5 (±0.3)	2.5 (±0.3)[11]
CTAB	1.2 (±0.3)	2.0 (±0.3)[11]

diffusion coeffcient as obtained from experiment includes contribution from both rotational and translational motion of the whole micelle, as discussed in refs 11 and 12. This justifies the fact that the values of the global diffusion coefficient from experiment are slightly higher than diffusion coefficients obtained from MSD curves.

Segmental MSD. The dynamical model derived from QENS data of SDS and C_nTAB micelles[9−11] describes hydrogen atoms belonging to CH_2 units moving in successively bigger spheres going from the headgroup to the tail, which is in apparent agreement with the results shown in Figure 4 for radial distance distributions. The experimental data can be compared with the MSD calculated from the global-motion-filtered trajectory, in order to highlight the local motion of the molecular units. Figure 6 shows the MSD for different

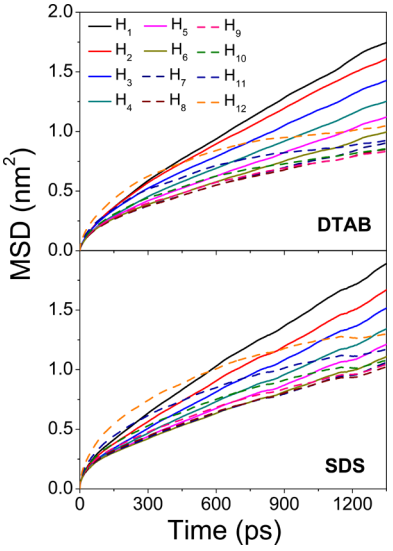

Figure 6. Segmental MSD as obtained from MD simulation for hydrogen atoms for SDS and DTAB micelles as a function of time.

segments of DTAB and SDS. In Figure 6, H_i correspond to hydrogen attached to carbon C_i. As can be seen from the figure, there exists a wide distribution of displacements of hydrogen atoms corresponding to different segments of the monomer. However, in contrast to the perceived image in which H_1 (hydrogen atoms closest to the headgroup) should have the smallest amplitude of motion and H_{12} (corresponding to the terminal CH_3 unit of the chain) should have the largest amplitudes of motion, both H_1 and H_{12} have comparably large

DOI: 10.1021/acs.jpcb.5b00020
J. Phys. Chem. B XXXX, XXX, XXX−XXX

amplitudes of motion, with the minimum amplitude being for the hydrogen atoms in the middle of the chain. The hydrophobic chains interact among themselves to form stable micelles, but the light, terminal tails are relatively mobile. The headgroups move despite their higher mass, because they are exposed to the solvent. A close correlation between solvent and solute (proteins, RNA, etc.) has been proposed on the basis of various experimental and simulation evidence.[39−41] Further, it has been argued that this correlation is purely solvent driven and does not depend much on the nature of the solute. This work shows the dynamics of surfactant molecules near the headgroup being mainly driven by the solvent irrespective of the polarity of the charged headgroups and their molecular form.

It is clear from the time dependence that the MSD of hydrogen atoms corresponding to the terminal part of the chain rises more quickly and tends to saturate in the course of the 2 ns production MD simulation, whereas the MSD of hydrogen atoms corresponding to molecular units closer to the headgroup rises more slowly but continuously, indicating slower dynamics and more volume occupied than by the tail. This difference in behavior results in a crossover of the MSDs of the heads and tails which occurs at ∼500 ps for SDS and 400 ps for DTAB. On the nanosecond time scale, the hydrogen atoms near the headgroups therefore have bigger amplitudes of motion than the terminal part of the tails. Taking into account the radial distance distributions of Figure 4, the headgroups must have a significant tangential, surface contribution to the MSD. The MSDs for the tails tend to saturate on the nanosecond time scale due to confinement mainly in the hydrophobic core. The analysis has been extended for SDS to 4 ns, and on this time scale, the headgroup motion tends to saturate at a value of ∼3 nm^2 (see the Supporting Information). Assuming the motion is tangential, the headgroups explore about one-seventh of the circumference of the micelle. Also of note is the fact that the MSDs of all the segments between the middle and the tail of the chains converge toward the same value of ∼1.5 nm^2, which is due to the tails being able to move from the center to the surface of the micelle and vice versa in several ns (see Figure 4).

The different dynamics of heads and tails can be seen more clearly from the MSDs on specific time scales, which corresponds to taking a vertical cut through the MSDs of Figure 6. The amplitude of displacements at 100 ps, corresponding to the energy resolution of the IRIS spectrometer, for the different hydrogen atoms (H_i) along the chain, have been calculated for SDS and shown in Figure 7a. Data calculated for different lengths of the equilibration simulation ranging from 10 to 75 ns are shown in the inset, which shows that 10 ns MD simulations are sufficient to equilibrate the micelle structure for SDS and therefore this equilibration time was used for DTAB, TTAB, and CTAB micelles (Figure 7b−d). Here, the error bar on the calculated amplitude of displacement is ∼±0.1 Å. It is evident from Figure 7 that there is an asymmetric U-shaped distribution of displacements of hydrogen atoms along the alkyl chain for all micelles, which depends on the time scale.

Amplitudes of displacement for the C_nTAB micelles are found to decrease with an increase in chain length n, as shown in Figure 7b, indicating that overall mobility decreases with an increase in n. The C_nTAB headgroups are in similar environments, yet longer chains reduce their mobility. Again, this is in accordance with our QENS results.[11] Taken

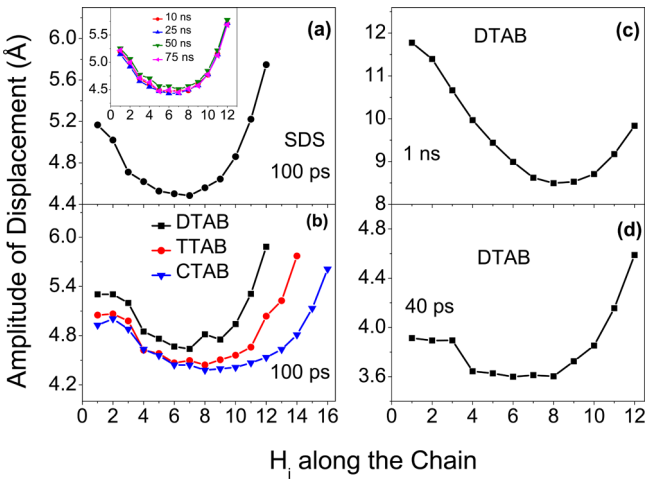

Figure 7. Variation of the amplitude of displacement of hydrogen atoms along the alkyl chain as obtained from MD simulation in (a) SDS micelles at 100 ps; the same for different equilibration run times is shown in the inset. (b) C_nTAB micelles having different chain lengths at 100 ps. (c) DTAB micelles at 1 ns and (d) DTAB micelles at 40 ps. The error bar on the calculated amplitude of displacement is ∼±0.1 Å.

collectively, these results on anionic and cationic micelles, in which the heads and tails, respectively, have been modified, indicate that the motion of heads and tails is strongly coupled. The asymmetry of the U-shaped segmental displacement is found to be reversed at 1 ns time scale compared to 40 ps, as shown in Figure 7c and d for DTAB micelles, corresponding to the crossover seen in Figure 4.

To validate the MD-based, structure-dynamics model against experimental data, the intermediate scattering functions $I(Q, t)$ as obtained from simulation (calculated for all hydrogen atoms) for SDS and DTAB micelles are shown in Figure 8a at a typical Q value of 1.0 Å^{-1}. $I(Q, t)$ can be analyzed with three processes and time scales corresponding to global, segmental, and torsional motions, as was done in the QENS experiment.[10] In a QENS experiment, the scattering function for segmental motion alone can be written as

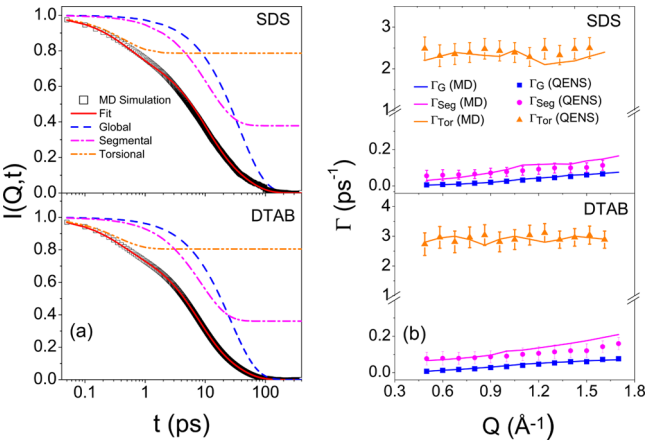

Figure 8. (a - left) Intermediate scattering function calculated from MD simulation for SDS and DTAB micelles at Q = 1.0 Å^{-1} at 300 K. (b - right) Decay constants (as described in eq 9) obtained from fitting of $I(Q, t)$ calculated from MD simulation or fitting of QENS spectra for both SDS and DTAB micelles.

DOI: 10.1021/acs.jpcb.5b00020
J. Phys. Chem. B XXXX, XXX, XXX−XXX

$$S_{seg}(Q, \omega) = A\delta(\omega) + (1 - A)L(\Gamma_{seg}, \omega) \quad (2)$$

The first term arises because of the localized nature of the motion and the constant A can be identified with the elastic incoherent structure factor (EISF), commonly used in quasielastic neutron scattering studies. The second term is the quasielastic component arising from the diffusive nature of the motion. $L(\Gamma_{seg}, \omega)$ is the Lorentzian with half width at half-maxima (HWHM), Γ_{seg}. In the time domain, eq 2 can be written as

$$I_{seg}(Q, t) = A + (1 - A)\exp(-\Gamma_{seg}t) \quad (3)$$

Similarly, for torsional motion, the scattering function can be written as

$$S_{Tor}(Q, \omega) = B\delta(\omega) + (1 - B)L(\Gamma_{Tor}, \omega) \quad (4)$$

B can be identified with the EISF for torsional motion, and in the time domain, the intermediate scattering function can be written as

$$I_{Tor}(Q, t) = B + (1 - B)\exp(-\Gamma_{Tor}t) \quad (5)$$

Similarly, the scattering function for the global motion in time and energy space can be written as

$$I_{Global}(Q, t) = \exp(-\Gamma_G t) \quad (6)$$

$$S_{Global}(Q, \omega) = L(\Gamma_{Global}, \omega) \quad (7)$$

When segmental, torsional, and global motion all are present, under the assumption that all of these are independent of each other, the total scattering function can be written as

$$S_{tot}(Q, \omega) = S_{Global}(Q, \omega) \otimes S_{Seg}(Q, \omega) \otimes S_{Tor}(Q, \omega) \quad (8)$$

Here, $\otimes$ signifies the convolution product. In the time domain, this can be written as

$$I_{tot}(Q, t) = [\exp(-\Gamma_G t)][A + (1 - A)\exp(-\Gamma_{Seg}t)][B + (1 - B)\exp(-\Gamma_{Tor}t)] \quad (9)$$

Γ's are the respective decay constants for the different motions and the constants A and B can be identified with the EISF for segmental and torsional motions, respectively. $I(Q, t)$ functions for the different components are shown in Figure 8a. The corresponding decay constants are shown in Figure 8b. To compare with the experimental results, the decay constants corresponding to the different motions are extracted from the QENS data from IRIS at ISIS and IN5 at ILL. The methodology adopted to extract the contribution pertaining to different dynamical motions using two spectrometers having different energy resolutions is discussed in ref 10. As can be seen in Figure 8b, the decay constants obtained from measurement and simulation are generally in good agreement, given that the experiments and simulations have been performed independently. None of the parameters in the force field have been adjusted to achieve this level of agreement. In particular, the global and torsional motions from experiment and simulation match closely, while there is a tendency for Γ_{seg} to be overestimated at high Q by 30% (DTAB) to 50% (SDS) by the simulations (see also Figure 9).

Further comparison for the segmental motion is based on the variation of decay constants with Q for different CH_2 units by assuming a suitable dynamical model. As indicated in Figure 7, the dynamical amplitudes of different hydrogen atoms of CH_2 units are smallest at the middle of the alkyl chain and increase for CH_2 units toward the head and tail ends of the molecules. A similar variation in diffusivities D for different hydrogen atoms along the alkyl chain is also expected. In this model, diffusivity of CH_2 units at the middle of the chain is a minimum (D_{min}) and increases to a maximum (D_{max}) toward the head and tail ends of the chain. As the total number of carbon atoms is 12 for SDS and DTAB, six independent CH_2 units with different diffusivity and amplitudes of motion are considered here. The scattering law in this case can be written, after modifying the Volino and Dianoux model,[42] as

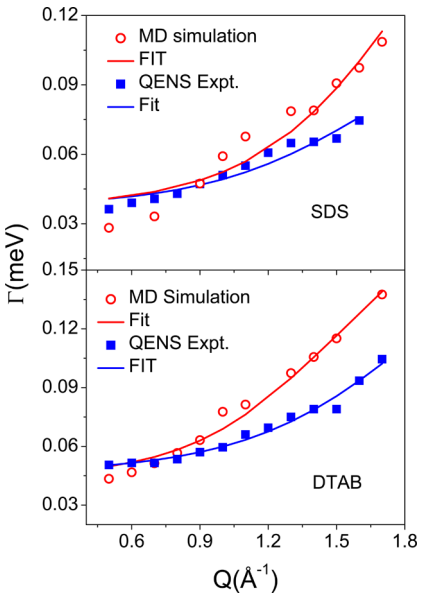

Figure 9. Variation of the decay constant, Γ_{seg}, obtained from QENS experiment and MD simulation which accounts for segmental motion of the monomer with Q for SDS and DTAB micelles. Solid lines represent the fit with the model discussed in the text.

$$S(Q, \omega) = \frac{1}{N}\sum_{i=1}^{N}\left[A_0^0(QR_i)\delta(\omega) + \frac{1}{\pi}\sum_{\{l,n\}\neq\{0,0\}}(2l + 1)A_n^l(QR_i)\frac{(x_n^l)^2 D_i/R_i^2}{[(x_n^l)^2 D_i/R_i^2]^2 + \omega^2}\right] \quad (10)$$

The first term corresponds to the elastic component, while the second term is the quasielastic component, which comprises a series of Lorentzians. $A_0^0(QR_i)$ and $A_n^l(QR_i)$ $(n, l \neq 0, 0)$ are the elastic and quasielastic structure factors. $A_n^l(QR)$ for different n and l can be calculated by using the values of x_n^l listed in ref 42. R_i and D_i are the radius of the sphere and associated diffusivity at the ith site of the alkyl chain, being minimum at the middle of the chain and increasing linearly and symmetrically toward the head and tail

$$R_i = \frac{i - 1}{N - 1}[R_{max} - R_{min}] + R_{min} \quad (11)$$

and

$$D_i = \frac{i - 1}{N - 1}[D_{max} - D_{min}] + D_{min} \quad (12)$$

where $N = 6$ for DTAB and SDS. A model of this kind has already been used by us to describe the QENS data where it

DOI: 10.1021/acs.jpcb.5b00020
J. Phys. Chem. B XXXX, XXX, XXX−XXX

Table 3. Radii of Spheres, R_{min} and R_{max}, and Associated Diffusion Coefficients, D_{min} and D_{max}, for the Alkyl Chain, as Obtained from the Least-Square Fitting of the MD Simulation and QENS Data with the Model Discussed in the Text

		R_{min} (Å)	R_{max} (Å)	D_{min} ($\times 10^{-5}$ cm^2/s)	D_{max} ($\times 10^{-5}$ cm^2/s)
SDS	MD simulation	0.5 ± 0.1	3.4 ± 0.3	0.5 ± 0.06	1.2 ± 0.2
	QENS experiment	0.4 ± 0.1	3.3 ± 0.2	0.1 ± 0.08	1.3 ± 0.2
DTAB	MD simulation	0.4 ± 0.1	4.1 ± 0.3	0.14 ± 0.07	1.7 ± 0.3
	QENS experiment	0.2 ± 0.1	3.0 ± 0.3	0.1 ± 0.05	1.3 ± 0.3

was assumed that the domain of dynamics and diffusivity varies linearly from the head to the tail of the alkyl chain.[9,10] The model described above, in which the diffusivity has a minimum for the middle of the chain, rather than at the headgroup, is equivalent, since this analysis does not impose the order in which the amplitudes vary along the molecule. The values of R_{min}, R_{max}, D_{min}, and D_{max} (eqs 10−12) obtained from simulation and experiment are given in Table 3. The variations of the decay constant for segmental motion with Q as obtained from MD simulation and QENS experiment are shown in Figure 9. The least-squares fits as obtained using the model described by eqs 10−12 are also shown.

As can be seen from Table 3, the values of R_{min} obtained from both MD simulation and QENS experiment are typically 0.2−0.5 Å, whereas the values of R_{max} are in the range 3.0−4.1 Å for SDS and DTAB micelles. It may be noted that these values are lower than those obtained directly from the MD trajectories, as reported in Figure 7. The asymmetric U-shaped amplitudes of displacement shown in Figure 7 are actually obtained from the global motion filtered MSDs. On the other hand, the dynamical parameters obtained from the least-squares fit of the $I(Q, t)$ do have the correlation effect due to the presence of different dynamical processes simultaneously. Therefore, the R_{min} and R_{max} obtained from the behavior of Γ_{seg} (Figure 9) suffer from this correlation effect.

The minimum diffusion coefficients for CH_2 units in the middle of the chain are in the range from 0.1 to 0.5 × 10^{-5} cm^2/s. The diffusion coefficients for CH_2 units at the head or tail end of the alkyl chain for SDS and DTAB micelles are in the range from 1.2 to 1.7 × 10^{-5} cm^2/s. The diffusivities obtained from simulation tend to be higher than those obtained from experiment due to the bigger values of Γ at high Q.

Overall, the agreement in the model parameters obtained from experimental and simulation data is satisfactory, resulting from similar values of Γ and the Q-dependences.

CONCLUSIONS

Detailed dynamical features of various ionic micelles have been investigated using molecular dynamics simulations and compared with neutron scattering data—the two independent approaches are consistent. Of the three types of motion—global motion of the whole micelle and segmental and fast torsional motion of the surfactants—we have focused on the segmental dynamics.

It is found that both heads and tails of surfactant monomers have a large mobility with a mobility minimum in the middle of the chain. The amplitude of the head motion is about 50% greater than that of the tails, the former having a dominant surface contribution, while the latter results from motion inside the micelle and excursions from the inside to the surface and back. At short times (<100 ps), the amplitude of motion of the tails is greater than that of the heads and this dynamical order is inverted at longer times (>500 ps).

Despite different headgroups and tail lengths, similar behavior is observed for all the ionic micelles, indicating the universal character of the dynamics. This observation is in contrast with the perceived image of micelle dynamics: heavy, relatively static headgroups and light, mobile tails. In essence, the "hydrophobic glue" which holds the micelle together is most effective in the middle regions of the chains, while the headgroups and tails, to a lesser extent, are exposed to the solvent. The key result from this study relating to the function of micelles is that the surfaces of micelles are rough and fluctuating, involving mobile headgroups and some tails. This increases the reactivity of the micellar surface, which is where most relevant processes are initiated.

This work demonstrates the added value of combining experiment and simulation, and future work will focus on implementing more accurate dynamical models from simulations in spectral analysis.

ASSOCIATED CONTENT

Supporting Information

Shape fluctuation of the micelle with time and global motion filtered mean square displacement as obtained from a long production run (4 ns). This material is available free of charge via the Internet at http://pubs.acs.org.

AUTHOR INFORMATION

Corresponding Author

*E-mail: mukhop@barc.gov.in. Phone: +91-22-25593754. Fax: +91-22-25505151.

Notes

The authors declare no competing financial interest.

REFERENCES

(1) Rosen, M. J.; Kunjappu, J. T. *Surfactants and Interfacial Phenomena*; John Wiley & Sons: Hoboken, NJ, 2012.

(2) Gerelli, Y.; Di Bari, M. T.; Barbieri, S.; Sonvico, F.; Colombo, P.; Natali, F.; Deriu, A. Flexibility and Drug Release Features of Lipid/Saccharide Nanoparticles. *Soft Matter* **2010**, *6*, 685−691.

(3) Verma, G.; Aswal, V. K.; Kulshreshtha, S. K.; Hassan, P. A.; Kaler, E. W. Adsorbed Anthranilic Acid Molecules Cause Charge Reversal of Nonionic Micelles. *Langmuir* **2008**, *24*, 683−687.

(4) Roberts, M. F.; Redfield, A. G. High-Resolution 31P Field Cycling NMR as a Probe of Phospholipid Dynamics. *J. Am. Chem. Soc.* **2004**, *126*, 13765−13777.

(5) Bratt, P. J.; Gillies, D. G.; Sutcliffe, L. H.; Williamst, A. J. NMR Relaxation Studies of Internal Motions: A Comparison Between micelles and Related Systems. *J. Phys. Chem.* **1990**, *94*, 2727−2729.

(6) Mahata, A.; Sarkar, D.; Bose, D.; Ghosh, D.; Girigoswami, A.; Das, P.; Chattopadhyay, N. Photophysics and Rotational Dynamics of a β-Carboline Analogue in Nonionic Micelles: Effect of Variation of Length of the Headgroup and the Tail of the Surfactant. *J. Phys. Chem. B* **2009**, *113*, 7517−7526.

(7) Bockstaele, M. V.; Gelan, J.; Martens, H.; Put, J.; Schryver, F-C. D.; Dederen, J. C. Occurrence of Chain folding in Micelles: A ^{13}C NMR Relaxation and Photophysical Study. *Chem. Phys. Lett.* **1980**, *70*, 605−609.

DOI: 10.1021/acs.jpcb.5b00020
J. Phys. Chem. B XXXX, XXX, XXX−XXX

(8) Bée, M. *Quasielastic Neutron Scattering*; Adam Hilger: Bristol, U.K., 1988.
(9) Sharma, V. K.; Mitra, S.; Verma, G.; Hassan, P. A.; Sakai, V. G.; Mukhopadhyay, R. Internal Dynamics in SDS Micelles: Neutron Scattering Study. *J. Phys. Chem. B* **2010**, *114*, 17049−17056.
(10) Sharma, V. K.; Mitra, S.; Sakai, V. G.; Hassan, P. A.; Embs, J. P.; Mukhopadhyay, R. The Dynamical Landscape in CTAB Micelles. *Soft Matter* **2012**, *8*, 7151−7160.
(11) Sharma, V. K.; Mitra, S.; Sakai, V. G.; Mukhopadhyay, R. Dynamical Features in Cationic Micelles of Varied Chain Length. *J. Phys. Chem. B* **2012**, *116*, 9007−9015.
(12) Sharma, V. K.; Mitra, S.; Johnson, M.; Mukhopadhyay, R. Dynamics in Anionic Micelles: Effect of Phenyl Ring. *J. Phys. Chem. B* **2013**, *117*, 6250−6255.
(13) Castelletto, V.; Hamley, I.W.; Yang, Z.; Haeussler, W. Neutron Spin-echo Investigation of the Dynamics of Block Copolymer Micelles. *J. Chem. Phys.* **2003**, *119*, 8158−8161.
(14) Doxastakis, M.; Sakai, V. G.; Ohtake, S.; Maranas, J. K.; Pablo, J. J. de. A Molecular View of Melting in Anhydrous Phospholipidic Membranes. *Biophys. J.* **2007**, *92*, 147−161.
(15) Busch, S.; Smuda, C.; Pardo, L. C.; Unruh, T. Molecular Mechanism of Long-Range Diffusion in Phospholipid Membranes Studied by Quasielastic Neutron Scattering. *J. Am. Chem. Soc.* **2010**, *132*, 3232−3233.
(16) Rheinstädter, M. C.; Das, J.; Flenner, E. J.; Brün-ing, B.; Seydel, T.; Kosztin, I. Motional Coherence in Fluid Phospholipid Membranes. *Phys. Rev. Lett.* **2008**, *101*, 248106-1−248106-4.
(17) Gerelli, Y.; Sakai, V. G.; Ollivier, J.; Deriu, A. Conformational and Segmental Dynamics in Lipid-based Vesicles. *Soft Matter* **2011**, *7*, 3929−3935.
(18) Marrink, S. J.; Tieleman, D. P.; Mark, A. E. Molecular Dynamics Simulation of the Kinetics of Spontaneous Micelle Formation. *J. Phys. Chem. B* **2000**, *104*, 12165−12173.
(19) Mohan, G.; Kopelevich, D. I. A Multiscale Model for Kinetics of Formation and Disintegration of Spherical Micelles. *J. Chem. Phys.* **2008**, *128*, 044905-1−044905-16.
(20) Dahirel, V.; Ancian, B.; Jardat, M.; Meriguet, G.; Turq, P.; Lequin, O. What Can be Learnt from the Comparison of Multiscale Brownian Dynamics Simulations, Nuclear Magnetic Resonance and Light Scattering Experiments on Charged Micelles. *Soft Matter* **2010**, *6*, 517−525.
(21) Volkov, N. A.; Divinskiy, B. B.; Vorontsov-Velyaminov, P. N.; Shchekin, A. K. Diffusivities of Species in Ionic Micellar Solutions: Molecular Dynamic Simulation. *Colloids Surf., A* **2014**, DOI: 10.1016/j.colsurfa.2014.10.030.
(22) Mackereel, A. D., Jr. Molecular Dynamics Simulation Analysis of a Sodium Dodecyl Sulfate Micelle in Aqueous Solution: Decreased Fluidity of the Micelle Hydrocarbon Interior. *J. Phys. Chem.* **1995**, *99*, 1846−1855.
(23) Bruce, C. D.; Berkowitz, M. L.; Perera, L.; Forbes, M. D. E. Molecular Dynamics Simulation of Sodium Dodecyl Sulfate Micelle in Water: Micellar Structural Characteristics and Counterion Distribution. *J. Phys. Chem. B* **2002**, *106*, 3788−3793.
(24) Cata, G. F.; Rojas, H. C.; Gramatges, A. P.; Zi-covich-Wilson, C. M.; Alvarez, L. J.; Searle, C. Initial Structure of Cetyltrimethylammonium Bromide Micelles in Aqueous Solution from Molecular Dynamics Simulations. *Soft Matter* **2011**, *7*, 8508−8515.
(25) Palazzesi, F.; Calvaresi, M.; Zerbetto, F. A Molecular Dynamics Investigation of Structure and Dynamics of SDS and SDBS Micelles. *Soft Matter* **2011**, *7*, 9148−9156.
(26) Sammalkorpi, M.; Karttunen, M.; Haataja, M. Structural Properties of Ionic Detergent Aggregates: A Large-Scale Molecular Dynamics Study of Sodium Dodecyl Sulfate. *J. Phys. Chem. B* **2007**, *111*, 11722−11733.
(27) Bogusz, S.; Venable, R. M.; Pastor, R. W. Molecular Dynamics Simulations of Octyl Glucoside Micelles: Dynamic Properties. *J. Phys. Chem. B* **2001**, *105*, 8312−8321.
(28) Venable, R. M.; Zhang, Y.; Hardy, B. J.; Pastor, R. W. Molecular Dynamics Simulations of a Lipid Bilayer and of Hexadecane: An Investigation of Membrane Fluidity. *Science* **1993**, *262*, 223−226.
(29) Flenner, E.; Das, J.; Rheinstädter, M. C.; Kosztin, I. Subdiffusion and Lateral Diffusion Coefficient of Lipid Atoms and Molecules in Phospholipid Bilayers. *Phys. Rev. E* **2009**, *79*, 011907-1−011907-11.
(30) Das, J.; Flenner, E.; Kosztin, I. Anomalous Diffusion of Water Molecules in Hydrated Lipid Bilayers. *J. Chem. Phys.* **2013**, *139*, 065102.
(31) Ollivier, J.; Mutka, H. IN5 Cold Neutron Time-of-Flight Spectrometer, Prepared to Tackle Single Crystal Spectroscopy. *J. Phys. Soc. Jpn.* **2011**, *80*, SB003-1−SB003-6.
(32) Campbell, S. I.; Telling, M. T. F.; Carlile, C. J. The Optimisation of Analyser Geometry in Near-Backscattering Spectrometers − IRIS on the ISIS-Pulsed Source. *Physica B* **2000**, *276−278*, 206−207.
(33) Berr, S. S. Solvent Isotope Effects on Alkytrimethylammonium Bromide Micelles as A Function of Alkyl Chain Length. *J. Phys. Chem.* **1987**, *91*, 4760−4765.
(34) Turro, N. J.; Yekta, A. Luminescent Probes for Detergent Solutions. A Simple Procedure for Determination of the Mean Aggregation Number of Micelles. *J. Am. Chem. Soc.* **1978**, *100*, 5951−5952.
(35) Phillips, J. C.; Braun, R.; Wang, W.; Gumbart, J.; Tajkhorshid, E.; Villa, E.; Chipot, C.; Skeel, R. D.; Kale, L.; Schulten, K. Scalable Molecular Dynamics with NAMD. *J. Comput. Chem.* **2005**, *26*, 1781−1802.
(36) MacKerell, A. D., Jr.; Feig, M.; Brooks, C. L., III. Extending the Treatment of Backbone Energetics in Protein Force Fields: Limitations of Gas-phase Quantum Mechanics in Reproducing Protein Conformational Distributions in Molecular Dynamics Simulations. *J. Comput. Chem.* **2004**, *25*, 1400−1415.
(37) Róg, T.; Murzyn, K.; Hinsen, K.; Kneller, G. R. *n*Moldyn: A Program Package for a Neutron Scattering Oriented Analysis of Molecular Dynamics Simulations. *J. Comput. Chem.* **2003**, *24*, 657−667.
(38) Kneller, G. R. Quasielastic Neutron Scattering and Relaxation Processes in Proteins: Analytical and Simulation-based Models. *Phys. Chem. Chem. Phys.* **2005**, *7*, 2641−2655.
(39) Chen, S.-H.; Liu, L.; Fratini, E.; Baglioni, P.; Faraone, A.; Mamontov, E. Observation of Fragile-to-Strong Dynamic Crossover in Protein Hydration Water. *Proc. Natl. Acad. Sci. U. S. A.* **2006**, *103*, 9012−9016.
(40) Tarek, M.; Tobias, D. J. Role of Protein-Water Hydrogen Bond Dynamics in the Protein Dynamical Transition. *Phys. Rev. Lett.* **2002**, *88*, 138101-1−138101-4.
(41) Wood, K.; Frolich, A.; Paciaroni, A.; Moulin, M.; Hartlein, M.; Zaccai, G.; Tobias, D. J.; Weik, M. Coincidence of Dynamical Transitions in a Soluble Protein and Its Hydration Water: Direct Measurements by Neutron Scattering and MD Simulations. *J. Am. Chem. Soc.* **2008**, *130*, 4586−4587.
(42) Volino, F.; Dianoux, A. J. Neutron Incoherent Scattering Law for Diffusion in a Potential of Spherical Symmetry: General Formalism and Application to Diffusion Inside a Sphere. *Mol. Phys.* **1980**, *41*, 271−279.

DOI: 10.1021/acs.jpcb.5b00020
J. Phys. Chem. B XXXX, XXX, XXX−XXX